Hindawi
Journal of Applied Mathematics
Volume 2023, Article ID 3065357, 13 pages
https://doi.org/10.1155/2023/3065357

Research Article

Modeling and Analysis of Unsteady Casson Fluid Flow due to an Exponentially Accelerating Plate with Thermal and Solutal Convective Boundary Conditions

Mehari Fentahun Endalew[1] **and Subharthi Sarkar**[2]

[1]*Department of Mathematics, Debre Tabor University, Debre Tabor 272, Ethiopia*
[2]*Department of Mathematics, Banwarilal Bhalotia College, Asansol 713303, India*

Correspondence should be addressed to Mehari Fentahun Endalew; mehexf@gmail.com

Received 4 January 2023; Revised 17 May 2023; Accepted 17 June 2023; Published 24 June 2023

Academic Editor: Waqar A. Khan

We intend to analyze the consequence of considering thermal radiation on time-dependent flow of the Casson fluid due to an exponentially accelerated inclined surface along with thermal as well as solutal convective boundary conditions. Fundamental equations governing an isotropic incompressible radiative Casson fluid flow are defined through a set of linear partial differential equations, and exact solutions are derived by using the Laplace transform approach. The numerical findings, obtained using MATLAB software, are presented in graphical and tabular representations based on the obtained analytical solutions of the fundamental equations. This investigation shows that the increment in thermal radiation results in the increment in fluid velocity and temperature distribution including thermal and momentum boundary layer thicknesses. Most interestingly, increasing the mass transfer coefficient results in an increment in the species concentration, velocity profiles, and mass transfer rate. However, the fluid velocity diminishes near the plate upon the increase in plate inclination. The scientific community will benefit greatly from this work since the findings can serve as benchmark solutions using numerical approaches to solve fully nonlinear flow governing problems.

1. Introduction

The discipline of thermal science dealing with the production, conversion, utilization, and exchanging of energy in thermal form between physical and mechanical systems is known as heat transfer. In other words, it is a process of thermal energy transfer from one location to the other due to the temperature difference. Analogy to this process that concerns with the transport of mass from the highly concentrated area to the lowly concentrated area is known as mass transfer. Nowadays, studies on the heat-mass transport principles with an inclusion of non-Newtonian fluid flow have been widely taking the place around the world because of their many utilities in our day-to-day experiences. Heat and mass transfer problems form an integral aspect of most scientific and engineering applications which can be medical, physical, chemical, and biological aspects. The escalating interaction of computer-assisted and experimental research methods can be guided or directed to new findings. These new results approve realistic representations and their physical interpretation and augment their formerly restricted applications significantly. Most lately, Riaz et al. [1] discussed an examination of mass and heat transfer effects with Maxwell's fluid flow near a plate assumed to vertical. DPL model of mass-heat transfer in small channels has been investigated by Endalew and Sarkar [2], Endalew et al. [3], and Sarkar et al. [4].

In addition, industrial and space technology applications heavily rely on the inclusion of thermal radiation in heat transfer calculations. Physically speaking, radiation is the energy emission in the form of ionizing, energetic, moving subatomic particles. An everyday illustration of thermal radiation is the infrared radiation that an electric heater or radiator emits. It is commonly known that electromagnetic

waves are used to transfer heat in this manner. Temperature differences between the surfaces and the range frequency of the energy being delivered and received can be used to visualize this form of heat transfer. For instance, sunlight contains energy from the visible, ultraviolet, and infrared spectrum. Research on the effects of thermal radiation on turbulent fluid flow across a slanted plate has been covered in Ref. [5–8]. Sobamowo et al. [9] have investigated the impact of heat radiation on fluid flow of the non-Newtonian type.

The Casson fluid is a word used to describe a piece of non-Newtonian fluid with changing viscosity. Due to the presence of varying viscosity in this kind of fluid, viscous force dominates the system. Paints, various polymer solutions, blood, honey, and other substances are examples of this fluid that are frequently used. Nandeppanavar [10] studied the flow of the Casson fluid over a plate in motion. Zaib et al. [11] investigated non-Newtonian Casson fluid flow through a permeable plate including heat transfer characteristics. The Casson fluid flow on the surface of the plate is investigated by Hayat et al. [12]. The effect of a Casson fluid entity on fluid flow has been extensively performed by Hussanan et al. [13]. The examination of the Casson fluid flow across the surface which is stretching has been discussed by Sheikh et al. [14]. Ahmad et al. [15] proposed an innovative method for simulating a Casson fluid using fractional derivative more recently. A Casson fluid flow was analyzed via similarity analysis to convert fundamental equations and partial differential equations into linear ordinary differential equations [16]. Additionally, studies describing the flow of the Casson fluid in different geometric configurations are carried out by Sarkar and Endalew [17, 18], Hamid et al. [19], Das et al. [20], Amjad et al. [21], Sarkar et al. [22], and so on.

As evident from the previous studies, the majority of researchers have taken either oscillating or linearly accelerating plates into consideration in their research. On the other hand, the idea of an exponentially accelerating plate has many wonderful uses in science and engineering. As a result, the flow over an exponential plate is considered in this research. A thermally inclined plate with simultaneous chemical reaction and thermal radiation has been used to perform mass and heat transfer impacts on time-varying flow that has been studied by Pattnaik et al. [23]. Additionally, numerous situations are included, and the fluid flow caused by an exponentially accelerating plate is examined in Refs. [24, 25].

Boundary conditions at the plate's wall, viz., thermal boundary condition and solutal boundary condition, are additional crucial mechanisms that can be very helpful in the research of mass-heat transfer fields. Many real-world scenarios have assumed that the movement of mass and heat from a body's surface is proportional to the surrounding surface temperature and the concentration of the surrounding walls. As a result, conjugate convective flow is another name for fluid flow. Using thermal and convective boundary conditions, Nandeppanavar et al. [26] investigated the Casson fluid flow with heat and mass transfer over a moving plate. Awais et al. [27] explored Newtonian heating and conjugate parameters for concentration on non-Newtonian fluid flows caused by a stretched surface. Rajesh [28] studied the effects of a thermal convective boundary condition and an impulsively launched infinite vertical plate on fluid flow. Solutions of mixed convective flow problems via numerically and analytically are obtained by Qasim et al. [29].

We believe that no research has been done on the time-dependent radiative Casson fluid flow caused by an exponentially accelerating inclined plate in the presence of thermal and solutal convective boundary conditions based on our rigorous examination of the aforementioned studies. By investigating the impact of convective boundary conditions on the time-dependent, incompressible, isotropic radiative Casson fluid flow brought on by an exponentially accelerating slanted vertical plate, this paper seeks to fill the knowledge gap. A solutal convective boundary condition for species concentration is additionally proposed in this scenario. Using the set of linear partial differential equations, the fluid flow model is constructed. The Laplace transform method is used for converting these equations into ordinary differential equations, which are then solved analytically. Closed-form solutions have been calculated for the fluid temperature, velocity, and species concentration. Utilizing graphs and tables, several mechanical variables affecting the features of fluid flow are examined, discovered, and debated. The scientific community will benefit from the findings of this work, which can also be used as a point of reference against which for the use of numerical techniques to address fully nonlinear governing problems.

2. Formulation of the Problem

This work considers the unsteady isotropic incompressible radiative Casson fluid flow across a tilted exponentially accelerating plate. Also, thermal and solutal convective boundary conditions are presumed here. Additionally, it is expected that the x'- and y'-axes are oriented vertically and horizontally, respectively. Furthermore, a random inclination of the plate by the angle α is asumed to be in the direction of flow. The temperature of the fluid and mass distribution far away from the plate are specified as T_∞ and C_∞, respectively. The plate is held stationary at $t' = 0$ and then at time $t' > 0$; then, it begins to move by the velocity $q = q_o \exp(a't')$ in self-plane with a constant velocity of q_o. Furthermore, the relationship between temperature and concentration levels and time is linear. The nature of the problem is represented in Figure 1.

"For an isotropic and incompressible Casson fluid flow, the rheological equation can be obtained from" (Ref. [30–32]) and expressed as follows:

$$\tau_{i,j} = \begin{cases} 2\left(\mu_b + \dfrac{P_y}{\sqrt{2\pi}}\right)e_{i,j} \text{ as } \pi_c < \pi, \\ 2\left(\mu_b + \dfrac{P_y}{\sqrt{2\pi_c}}\right)e_{i,j} \text{ as } \pi_c > \pi. \end{cases} \tag{1}$$

From the above, $\tau_{i,j}$ represents stress tensor components, $e_{i,j}$ specifies fluid deformation rate, π symbolizes self-

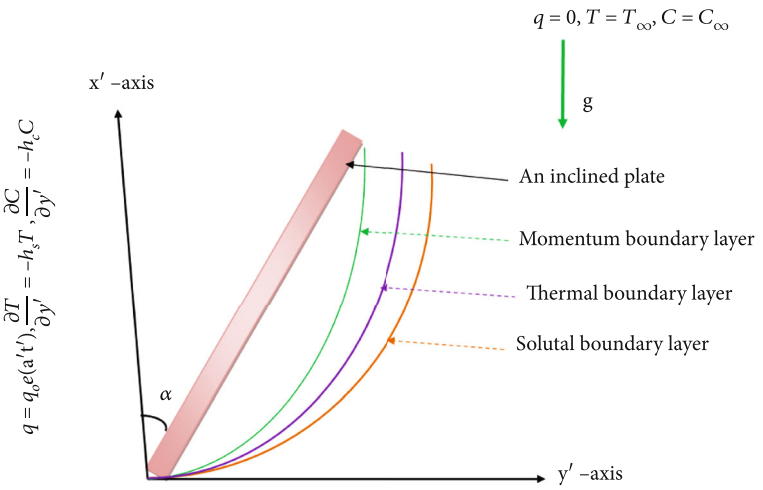

Figure 1: Geometrical representation of the problem.

product of strain tensor rate, π_c denotes critical value of the strain tensor's rate as a function of itself, P_y represents yield stress, and μ_b is a dynamic plastic viscosity.

We know that $\pi = e_{i,j}e_{i,j}$. As a result, the fluid exhibits a solid behavior when subjected to shear stresses that are lower than yield stresses, whereas it starts moving as yield stress smaller than shear stress.

The governing equations and initial and boundary conditions are therefore given, together with the aforementioned physical assumptions as follows (see Refs. [13, 27, 32]):

$$\frac{\partial q}{\partial t'} - \nu\left(1 + \frac{1}{\beta}\right)\frac{\partial^2 q}{\partial y'^2} = g(\cos\alpha)[\beta_C(C - C_\infty) + \beta_T(T - T_\infty)], \tag{2}$$

$$\rho C_p \frac{\partial T}{\partial t'} + \frac{\partial q_r}{\partial y'} = \kappa \frac{\partial^2 T}{\partial y'^2}, \tag{3}$$

$$\frac{\partial C}{\partial t'} = D_m \frac{\partial^2 C}{\partial y'^2}. \tag{4}$$

Mathematically, equations (2), (3), and (4) are called momentum, heat or diffusion, and mass or concentration equations, respectively.

The initial and boundary conditions are as follows [33]:

$$q\left(y', 0\right) = 0, C\left(y', 0\right) = C_\infty, T\left(y', 0\right) = T_\infty, \forall y', \tag{5a}$$

$$q\left(0, t'\right) = q_o \exp\left(\left(a't'\right)\right), \frac{\partial T\left(0, t'\right)}{\partial y'} = -h_f T\left(0, t'\right), \frac{\partial C\left(0, t'\right)}{\partial y'} = -k_f C\left(0, t'\right), \tag{5b}$$

$$q\left(\infty, t'\right) \longrightarrow 0, T\left(\infty, t'\right) \longrightarrow T_\infty, C\left(\infty, t'\right) \longrightarrow C_\infty \text{ at } t' > 0. \tag{5c}$$

The Rosseland approximation for radiation heat flow is considered since an optically thick fluid is being taken into account (see Refs. [34, 35]) and written as follows:

$$q_r = -\frac{4\sigma}{c^*}\frac{\partial T^4}{\partial y'}, \tag{6}$$

where c^* defines the constant of absorption and σ symbolizes the constant of Stefan-Boltzmann.

It is thought that there is relatively low temperature change throughout the fluid movement. Thus, T^4 can be expressed as fluid temperature distribution in the flow system. We are left with the following equation after performing the expansion of the Taylor series of $T'4$ about T_∞' and discarding its highest order:

$$T^4 \cong 4TT_\infty^3 - 3T_\infty^4. \tag{7}$$

Substitute equations (6) and (7) in (3) to get

$$\rho C_p \frac{\partial T}{\partial t'} = \kappa\left(1 + \frac{16\sigma T_\infty}{3c^*\kappa}\right)\frac{\partial^2 T}{\partial y'^2}. \tag{8}$$

To reduce aforementioned equations to dimensionless, the following dimensionless physical quantities and parameters have been assumed:

$$\left.\begin{aligned} t &= \frac{t'q_o^2}{\nu}, y = \frac{y'q_o}{\nu}, u = \frac{q}{q_o}, \mathrm{Gr} = \frac{\nu g\beta_T(T_\infty)}{q_o^3}, \gamma = \frac{h_f\nu}{q_o}, \\ \mathrm{Gm} &= \frac{\nu g\beta_C(C_\infty)}{q_o^3}, \theta = \frac{T - T_\infty}{T_\infty}, a = \frac{a'\nu^2}{q_o^2}, \eta = \frac{k_f\nu}{q_o}, \\ \phi &= \frac{C - C_\infty}{C_\infty}, R = \frac{16\sigma T_\infty^3}{c^*\kappa}, P_r = \frac{\mu C_p}{\kappa}, \mathrm{Sc} = \frac{\nu}{D}. \end{aligned}\right\} \tag{9}$$

Therefore, the reduced dimensionless form of equations (2), (4), and (8) is as follows:

$$\frac{\partial u}{\partial t} = \left(1 + \frac{1}{\beta}\right)\frac{\partial^2 u}{\partial y^2} + (\cos\alpha)Gr\theta + (\cos\alpha)\mathrm{Gm}\phi, \tag{10}$$

$$P_r\frac{\partial \theta}{\partial t} = (1+R)\frac{\partial^2 \theta}{\partial y^2}, \tag{11}$$

$$\mathrm{Sc}\frac{\partial \phi}{\partial t} = \frac{\partial^2 \phi}{\partial y^2}, \tag{12}$$

with the following dimensionless initial and boundary conditions:

$$u(y,0) = \theta(y,0) = \phi(y,0) = 0, \forall y, \tag{13a}$$

$$u(0,t) = e^{at}, \frac{\partial\theta(0,t)}{\partial y} = -\gamma(1+\theta(0,t)), \frac{\partial\phi(0,t)}{\partial y} = -\eta(1+\phi(0,t)), \tag{13b}$$

$$u(\infty,t) \longrightarrow 0, \theta(\infty,t) \longrightarrow 0, \phi(\infty,t) \longrightarrow 0 \text{ at } t > 0. \tag{13c}$$

3. Solution Method

A time function is converted into a frequency function using the Laplace transform mathematical approach. If we transform both sides of a differential equation, we can often solve the resulting equations with algebraic methods. The method entails to apply the Laplace transform on the time-dependent partial differential equations to transform them into time-independent but frequency-dependent ordinary differential equations in the Laplace domain, which are then transformed into algebraic equations. The final analytical solution is obtained by inverting the analytical solutions obtained in the Laplacian frequency domain into a final solution in temporal and spatial coordinates. That is here, the exact solutions of governing equations (10)-(12) with initial and boundary conditions ((13a)-(13c)) are evaluated by the well-known Laplace transform method. Therefore, first, we take the Laplace transform on both sides of all equations (10)-(12). Then, we use the initial conditions (13a) and make some rearrangement; the following transformed ordinary differential equations (ODEs) are obtained:

$$\frac{d^2\widehat{u}}{dy^2} = \lambda_1\left(su - \mathrm{Gr}\widehat{\theta}\cos\alpha - \mathrm{Gm}\widehat{\phi}\cos\alpha\right), \tag{14}$$

$$\frac{d^2\widehat{\theta}}{dy^2} = s\lambda\widehat{\theta}, \tag{15}$$

$$\frac{d^2\widehat{\phi}}{dy^2} = \mathrm{Sc}s\widehat{\phi}, \tag{16}$$

where $\lambda = \mathrm{Pr}/(1+R)$ and $\lambda_1 = \beta/(1+\beta)$.

The boundary conditions can be transformed as follows using a similar method:

$$\widehat{u} = \frac{1}{s-a}, \frac{d\widehat{\theta}}{dy} = -\gamma\left(\widehat{\theta} + \frac{1}{s}\right), \frac{d\widehat{\phi}}{dy} = -\eta\left(\widehat{\phi} + \frac{1}{s}\right), \tag{17a}$$

$$\widehat{u}(\infty,s) \longrightarrow 0, \widehat{\theta}(\infty,s) \longrightarrow 0, \widehat{\phi}(\infty,s) \longrightarrow 0. \tag{17b}$$

In order to get the Laplace domain solutions for mass and temperature fields, let us first solve equations (16) and (15) along with their boundary conditions. As a result, the solutions are provided as follows:

$$\widehat{\phi} = \frac{a_2}{s\left(\sqrt{s}-a_2\right)}e^{-y\sqrt{s\mathrm{Sc}}}, \tag{18}$$

$$\widehat{\theta} = \frac{b_1}{s\left(\sqrt{s}-b_1\right)}e^{-y\sqrt{s\lambda}}. \tag{19}$$

Equations (17a), (18), and (19) can then be used to solve equation (14), yielding the following fluid velocity solution:

$$\begin{aligned}\widehat{u} = {} & \frac{e^{-y\sqrt{s\lambda_1}}}{s-a} + \frac{\lambda_1 a_2 a_3}{s^2\left(\sqrt{s}-a_2\right)}\left(e^{-y\sqrt{s\lambda_1}} - e^{-y\sqrt{s\lambda}}\right) \\ & + \frac{\lambda_1 b_1 b_2}{s^2\left(\sqrt{s}-b_1\right)}\left(e^{-y\sqrt{s\lambda_1}} - e^{-y\sqrt{s\mathrm{Sc}}}\right),\end{aligned} \tag{20}$$

where $a_2 = \gamma/\sqrt{\lambda}$, $a_3 = \mathrm{Gr}\cos\alpha/(\lambda - \lambda_1)$, $b_1 = \eta/\sqrt{\mathrm{Sc}}$, and $b_2 = \mathrm{Gm}\cos\alpha/(\mathrm{Sc} - b_1)$.

The solutions for dimensionless velocity, distribution of temperature, and species concentration in dense structure are shown below, respectively. This is done by employing the Laplace inverse on equations ((18)-(20)) and then utilizing the straight-forward technique to generate an inverse Laplace transform with an exponential form and associated with error functions presented by Hetnarski [36, 37].

$$\begin{aligned}u = {} & H_1(y,t,a,\lambda_1) + \frac{\lambda_1 a_3}{a_2^2}\left[H_2\left(y\sqrt{\lambda_1},t,a_2\right) - H_2\left(y\sqrt{\lambda},t,a_2\right)\right] \\ & - \frac{\lambda_1 a_3}{a_2}\left[H_3\left(y\sqrt{\lambda_1},t\right) - H_3\left(y\sqrt{\lambda},t\right)\right] \\ & - \lambda_1 a_3\left[H_4\left(y\sqrt{\lambda_1},t\right) - H_4\left(y\sqrt{\lambda},t\right)\right] \\ & + \frac{\lambda_1 b_2}{b_1^2}\left[H_2\left(y\sqrt{\lambda_1},t,b_1\right) - H_2\left(y\sqrt{\mathrm{Sc}},t,b_1\right)\right] \\ & - \frac{\lambda_1 b_2}{b_1}\left[H_3\left(y\sqrt{\lambda_1},t\right) - H_3\left(y\sqrt{\mathrm{Sc}},t\right)\right] \\ & - \lambda_1 b_2\left[H_4\left(y\sqrt{\lambda_1},t\right) - H_4\left(y\sqrt{\mathrm{Sc}},t\right)\right].\end{aligned} \tag{21}$$

Likewise, the nondimensional temperature and concentration can be revealed as follows:

$$\theta = H_2\left(y\sqrt{\lambda},t,a_2\right), \tag{22}$$

$$\phi = H_2\left(y\sqrt{\mathrm{Sc}}, t, b_1\right). \tag{23}$$

The following definitions apply to the dummy functions H_1, H_2, H_3, and H_4, respectively:

$$\begin{aligned}
H_1(a,t,b,c) &= \frac{e^{bt}}{2}\left[e^{a\sqrt{b}}\ \mathrm{erf}\ c\left(\frac{a}{2}\sqrt{\frac{c}{t}}+\sqrt{\frac{bt}{c}}\right)\right.\\
&\quad \left. + e^{-a\sqrt{b}}\ \mathrm{erf}\ c\left(\frac{a}{2}\sqrt{\frac{c}{t}}-\sqrt{\frac{bt}{c}}\right)\right],\\
H_2(a,t,b) &= e^{\left(b^2t-ab\right)}\ \mathrm{erf}\ c\left(\frac{a}{2\sqrt{t}}-b\sqrt{t}\right)-\mathrm{erf}\ c\left(\frac{a}{2\sqrt{t}}\right),\\
H_3(a,t) &= 2\sqrt{\frac{t}{\pi}}e^{-a^2/4t}-a\ \mathrm{erf}\ c\left(\frac{a}{2\sqrt{t}}\right),\\
H_4(a,t) &= \left(\frac{a^2}{2}+t\right)\mathrm{erf}\ c\left(\frac{a}{2\sqrt{t}}\right)-a\sqrt{\frac{t}{\pi}}e^{-a^2/4t},\\
H_5(a,t) &= \mathrm{erf}\ c\left(\frac{a}{2\sqrt{t}}\right).
\end{aligned} \tag{24}$$

4. Surface-Based Dimensionless Coefficients

A few surface-based dimensionless coefficients that may be essential in the investigation of viscous fluid dynamics are skin friction, Sherwood's number, and Nusselt's number. Equations (21) through (23), which determine these surface coefficients in this instance, are then used to explicitly articulate and analyze them as follows:

4.1. Skin Friction Coefficient. It is denoted by the symbol τ, which is a dimensionless quantity that is caused by the motion fluid acting on the plate's surface. This amount is calculated using equation (21) and is stated as follows:

$$\begin{aligned}
\tau &= -\left(1+\frac{1}{\beta}\right)\left.\frac{\partial u(y,t)}{\partial y}\right|_{y=0}\\
&= \frac{1}{\lambda_1}P_1(a,t,\lambda_1)+a_3\left(\frac{\sqrt{\lambda_1}-\sqrt{\lambda}}{a_2}\right)[P_2(a_2,t)-1]\\
&\quad + 2a_3P_3(\lambda_1,t,\lambda)+b_2\left(\frac{\sqrt{\lambda_1}-\sqrt{Sc}}{b_1}\right)[P_2(b_1,t)-1]\\
&\quad + 2b_2P_3(\lambda_1,t,\mathrm{Sc})+\frac{1}{\lambda_1}\sqrt{\frac{\lambda_1}{\pi t}}.
\end{aligned} \tag{25}$$

4.2. Nusselt Number. The surface coefficient, abbreviated as Nu, is a dimensionless quantity that explains the heat transfer rate at the surface of the plate. It is calculated from equation (22) and provided as follows:

$$\mathrm{Nu} = -\left.\frac{\partial\theta(y,t)}{\partial y}\right|_{y=0} = a_2\sqrt{\lambda}P_2(a_2,t). \tag{26}$$

4.3. Sherwood Number. The mass transfer rate at the plate wall is controlled by a nondimensional variable known as the Sherwood number, abbreviated Sh. It is presented as follows and comes from equation (23):

$$\mathrm{Sh} = -\left.\frac{\partial\phi(y,t)}{\partial y}\right|_{y=0} = b_1\sqrt{\mathrm{Sc}}P_2(b_1,t). \tag{27}$$

The functions P_1, P_2, and P_3 are defined as follows:

$$\begin{aligned}
P_1(a,t,b) &= e^{at}\left[\sqrt{a}\left(1-\mathrm{erf}\ c\left(\sqrt{\frac{at}{b}}\right)\right)+\sqrt{\frac{b}{\pi t}}e^{-\frac{at}{b}}\right],\\
P_2(a,t) &= e^{a^2t}\left(2-\mathrm{erf}\ c\left(a\sqrt{t}\right)\right),\\
P_3(a,t,b) &= \sqrt{\frac{bt}{\pi}}-\sqrt{\frac{at}{\pi}}.
\end{aligned} \tag{28}$$

5. Restricting Scenarios of the Problem

In this occasion, the Laplace transform is employed to generate more general analytical results. Therefore, the restricting scenarios of the present investigation are provided below and explored in detail.

5.1. Newtonian Fluid Case. When we set $\beta \longrightarrow \infty$, equation (21) is reduced to the usual Newtonian fluid. Then, its solution can be expressed as follows:

$$\begin{aligned}
u(y,t) &= H_1(y,t,a,\lambda_1)+\frac{a_3}{a_2^2}\left[H_2(y,t,a_2)-H_2\left(y\sqrt{\lambda},t,a_2\right)\right]\\
&\quad -\frac{a_3}{a_2}\left[H_3(y,t)-H_3\left(y\sqrt{\lambda},t\right)\right]\\
&\quad -a_3\left[H_4(y,t)-H_4\left(y\sqrt{\lambda},t\right)\right]\\
&\quad +\frac{b_2}{b_1^2}\left[H_2(y,t,b_1)-H_2\left(y\sqrt{\mathrm{Sc}},t,b_1\right)\right]\\
&\quad -\frac{b_2}{b_1}\left[H_3(y,t)-H_3\left(y\sqrt{\mathrm{Sc}},t\right)\right]\\
&\quad -b_2\left[H_4(y,t)-H_4\left(y\sqrt{\mathrm{Sc}},t\right)\right].
\end{aligned} \tag{29}$$

The shearing stress for this case can be evaluated as well as follows:

$$\begin{aligned}
\tau &= -\left.\frac{\partial u(y,t)}{\partial y}\right|_{y=0} = P_1(a,t,1)+a_3\left(\frac{1-\sqrt{\lambda}}{a_2}\right)[P_2(a_2,t)-1]\\
&\quad + 2a_3P_3(1,t,\lambda)+b_2\left(\frac{1-\sqrt{\mathrm{Sc}}}{b_1}\right)[P_2(b_1,t)-1]\\
&\quad + 2b_2P_3(1,t,\mathrm{Sc})+\sqrt{\frac{1}{\pi t}}.
\end{aligned} \tag{30}$$

5.2. Absence of Natural Convection. Equation (21) becomes simpler when the free convection terms are removed, i.e., Gr = Gm = 0.

$$u(y,t) = H_1(y,t,a,\lambda_1). \tag{31}$$

Similar to this, reduced skin friction with omitting of free convection term is provided as follows:

$$\tau = -\left(1+\frac{1}{\beta}\right)\left.\frac{\partial u(y,t)}{\partial y}\right|_{y=0} = \frac{1}{\lambda_1}\left[P_1(a,t,\lambda_1) + \sqrt{\frac{\lambda_1}{\pi t}}\right]. \tag{32}$$

5.3. Flow over an Accelerating Plate. If we make $a = 0$ in equation (21), the flow problem is naturally reduced into fluid flow due to an impulsively accelerating plate. In this line, the solution of velocity is stated as follows:

$$\begin{aligned} u(y,t) = {} & H_5\left(y\sqrt{\lambda_1},t\right) + \frac{\lambda_1 a_3}{a_2^2}\left[H_2\left(y\sqrt{\lambda_1},t,a_2\right) - H_2\left(y\sqrt{\lambda},t,a_2\right)\right] \\ & - \frac{\lambda_1 a_3}{a_2}\left[H_3\left(y\sqrt{\lambda_1},t\right) - H_3\left(y\sqrt{\lambda},t\right)\right] \\ & - \lambda_1 a_3\left[H_4\left(y\sqrt{\lambda_1},t\right) - H_4\left(y\sqrt{\lambda},t\right)\right] \\ & + \frac{\lambda_1 b_2}{b_1^2}\left[H_2\left(y\sqrt{\lambda_1},t,b_1\right) - H_2\left(y\sqrt{\mathrm{Sc}},t,b_1\right)\right] \\ & - \frac{\lambda_1 b_2}{b_1}\left[H_3\left(y\sqrt{\lambda_1},t\right) - H_3\left(y\sqrt{\mathrm{Sc}},t\right)\right] \\ & - \lambda_1 b_2\left[H_4\left(y\sqrt{\lambda_1},t\right) - H_4\left(y\sqrt{\mathrm{Sc}},t\right)\right]. \end{aligned} \tag{33}$$

In this case, the skin friction can be expressed as follows:

$$\begin{aligned} \tau = {} & -\left(1+\frac{1}{\beta}\right)\left.\frac{\partial u(y,t)}{\partial y}\right|_{y=0} \\ = {} & \frac{1}{\lambda_1}P_1(0,t,\lambda_1) + a_3\left(\frac{\sqrt{\lambda_1}-\sqrt{\lambda}}{a_2}\right)[P_2(a_2,t)-1] \\ & + 2a_3P_3(\lambda_1,t,\lambda) + b_2\left(\frac{\sqrt{\lambda_1}-\sqrt{\mathrm{Sc}}}{b_1}\right)[P_2(b_1,t)-1] \\ & + 2b_2P_3(\lambda_1,t,\mathrm{Sc}) + \frac{1}{\lambda_1}\sqrt{\frac{\lambda_1}{\pi t}}. \end{aligned} \tag{34}$$

Using a graphical presentation and tabular format, numerical findings generated from analytical solutions of the most important equations governing fluid flow are given and discussed. We have employed MATLAB software to generate graphics and tables for numerical values of different physical parameters.

6. Validation of the Result

As it is known, the current result of the problem should be compared with the existing publication/experimental results in order to validate novel findings of this research work. In this line, when we avoid the free/natural convective terms and inclination angle, that is, $\alpha = \mathrm{Gr} = \mathrm{Gm} = 0$ from the solution of momentum/velocity equation, the momentum/velocity equation is the same as provided in by Hussanan et al. [13]. The solutions of both investigations (the current and previously published [13]) meet with excellent confirmation. Thus, the validation of the present finding is checked and confirmed.

7. Results and Discussion

In the current research, exact closed-form solutions to the basic equations governing the flow of radiative Casson fluid caused by an exponentially accelerating inclined plate are found by utilizing the Laplace transform method. Then, in order to validate the behaviors of the Casson fluid flow under various conditions, numerical values obtained from analytical expressions that determine the solution of the governing equations characterizing the fluid flow are described through figures and tables. If not otherwise indicated, the appropriate values for the significant physical entities in this case are to be allocated as $\mathrm{Gr} = \mathrm{Gm} = R = 1$, $\gamma = \eta = 0.6$, $\alpha = \pi/3$, $\mathrm{Pr} = 0.71$, $t = 1$, $\mathrm{Sc} = 0.6$, $\beta = 2$, and $a = 0.1$. A common trend has been perceived in all the velocity profiles for all values of flow parameters. It can be seen that the velocity profiles first increase uniformly near the surface, attain a maximum value, and then decrease uniformly throughout the boundary layer which eventually tends asymptotically to the zero velocity at the free stream. This trend is due to the fact that the plate starts moving from rest with an initial velocity which varies exponentially with time, and hence, due to no slip between the walls of the plate and the fluid, a fluid flow is generated near the plate. Thus, a boundary layer is also formed in the direction of the movement of the plate. Away from the plate fluid flow is impacted by the resting free stream. All this contribute to the nature of the fluid flow profiles as could be seen in the following figures. Therefore, mathematically, all such fluid flows are represented by complementary error functions whose graph rightfully resembles the fluid flow characteristics.

In this analysis, the free or natural convective aspect has been assumed and buoyant forces are induced into the fluid and discussed in detail. It should be emphasized that these forces result from density variations brought on by fluid temperature and concentration variations. This is due to the nature of buoyancy forces, specifically the thermal and solutal buoyant forces, which are connected to thermal and solutal Grashof numbers, through direct proportion. Thus, a rise in the Grashof number implies a rise in the buoyant forces which dominates other physical entities influencing the fluid flow characteristics. This in turn significantly enhances the fluid flow. Additionally, the effects of viscous force on the fluid are diminished due to the dominance of buoyant forces. As a result, when the Grashof numbers rise, the fluid velocity and the thickness of the momentum boundary layer increase, as depicted in Figures 2 and 3.

Figure 4 shows the influence of plate inclination on a Casson fluid velocity including the thickness of its boundary layer. Here, with an increment in the inclination angle of the

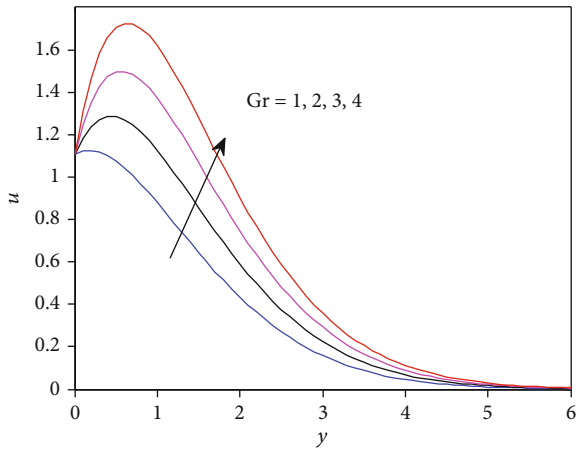

Figure 2: Thermal Grashof number impact on fluid velocity.

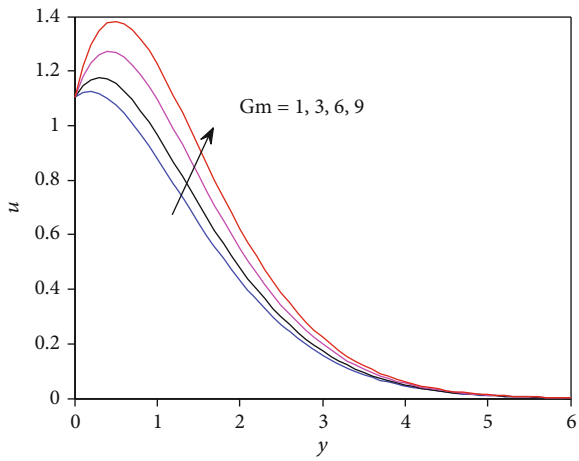

Figure 3: Solutal Grashof number effect on fluid velocity.

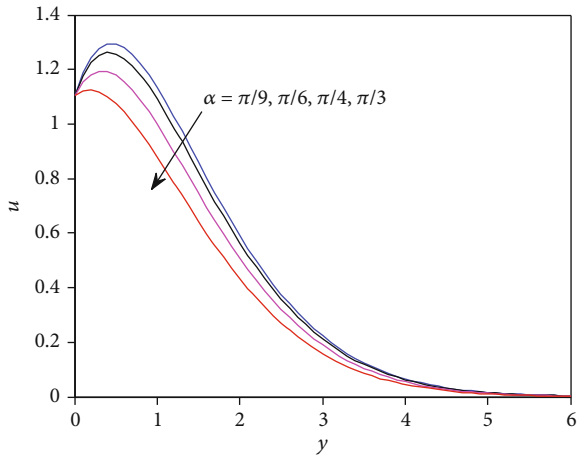

Figure 4: Plate inclination impact on fluid velocity.

plate, the mean velocity of the Casson fluid is reduced. This is due to the presence of high frictional force on the plate's surface as well as an augmented impact of buoyancy force. It is widely known that the force of friction exerting on a

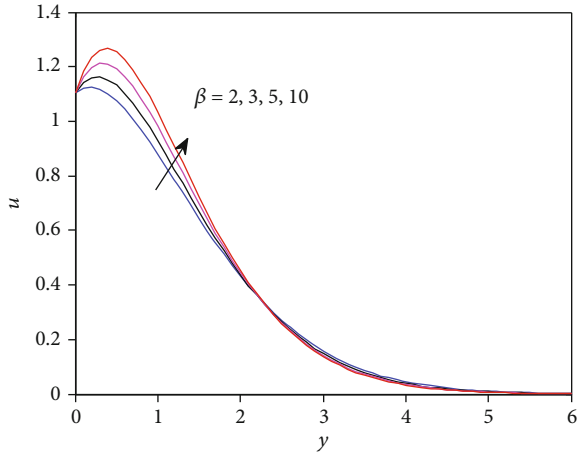

Figure 5: Effects of the Casson fluid parameter on fluid velocity.

fluid dramatically expands across the domain of fluid flow as the plate is inclined along the flow route by any arbitrary angle. Due to this physical reality, boundary layer thickness and fluid velocity are reduced (see Figure 4). Figure 5 explores one method by which the parameter of the Casson fluid influences the velocity of fluid. To replicate blood flow in narrow arteries, the Casson fluid model, a non-Newtonian fluid with a yield stress, is widely utilized. "The mathematical simulation of low-shear rate blood flow in constricted arteries has frequently used the Casson fluid model. The Casson fluid, a shear-thinning fluid, is supposed to have infinite viscosity at zero shear rates, zero viscosity at an infinite shear rate, and yield stress below which there is no flow" [31]. It should be emphasized that in the analysis of the Casson fluid flow, the viscous force has a significant impact on the fluid flow. However, as this parameter is raised, the viscous force diminishes. The velocity of the fluid and, hence, the momentum boundary layer thickness increase in size as the Casson fluid parameter rises.

It is noted that the Prandtl number physically expresses the ratio of the thermal diffusivity of a fluid to the viscous/frictional force acting on it. According to this justification, the fluid can become viscous force-dominated as the Prandtl number increases. In this line, as seen in Figure 6, the fluid velocity falls down as the Prandtl number grows up. Here, the values of Pr is considered for different fluids as Pr = 0.54 for noble gases with hydrogen, Pr = 0.71 for dry air, Pr = 0.91 for different gases, and Pr = 1.38 for ammonia. However, as indicated in Figure 7, as the Prandtl number rises, the temperature distribution falls. The reason for this is that thermal diffusivity and Prandtl's number have an inverse relationship. These two graphs demonstrate that as the value of Prandtl's number rises, the widths of the thermal and momentum boundary layers narrow down. The Schmidt number can be explained using similar arguments. Figures 8 and 9 demonstrate how it affects species concentration and fluid velocity. These data demonstrate that fluid velocity and fluid temperature distribution decrease both as the value Schmidt number increases. Thus, the thicknesses of the momentum boundary layer and the solutal boundary layer also decrease as solutal diffusion decreases.

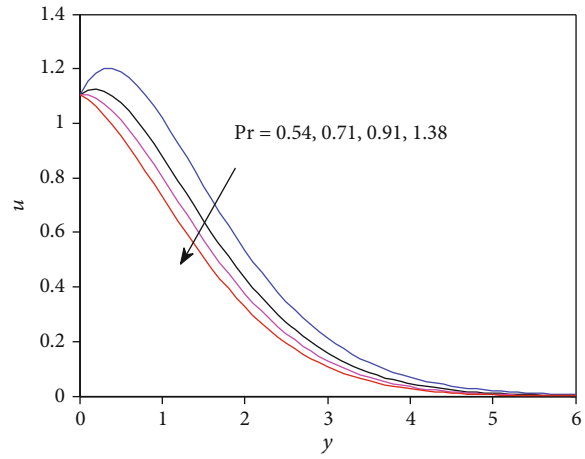

Figure 6: Impacts of the Prandtl number on fluid velocity.

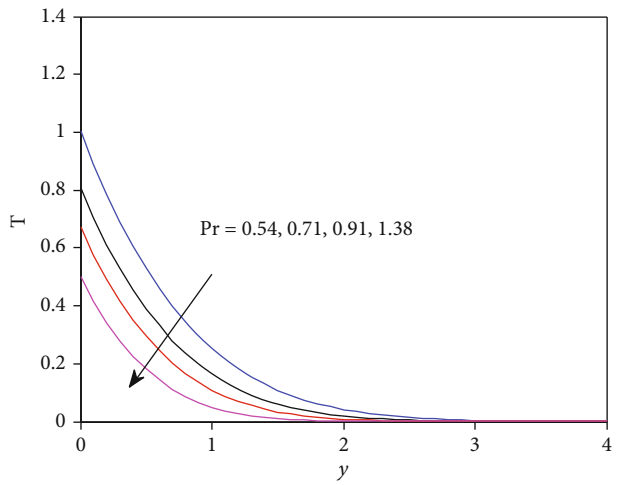

Figure 7: Influences of the Prandtl number on fluid temperature.

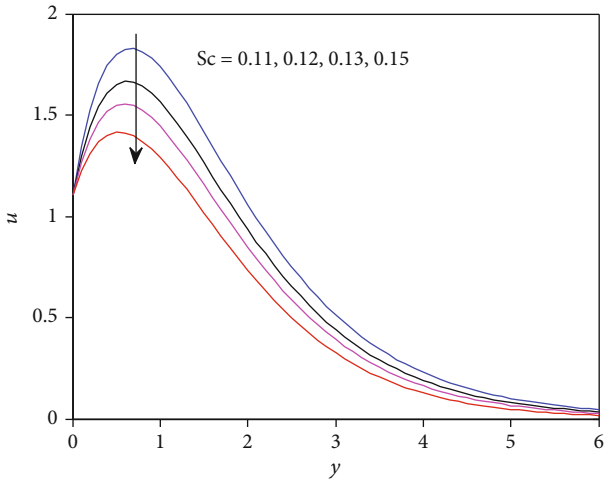

Figure 8: Influences of the Schmidt number on fluid velocity.

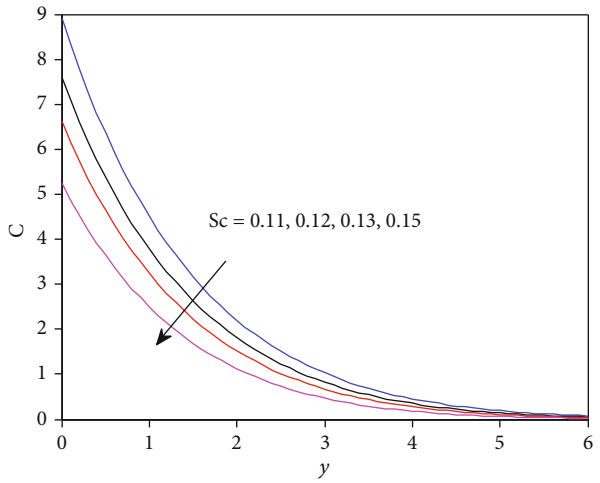

Figure 9: Influences of the Schmidt number on species concentration.

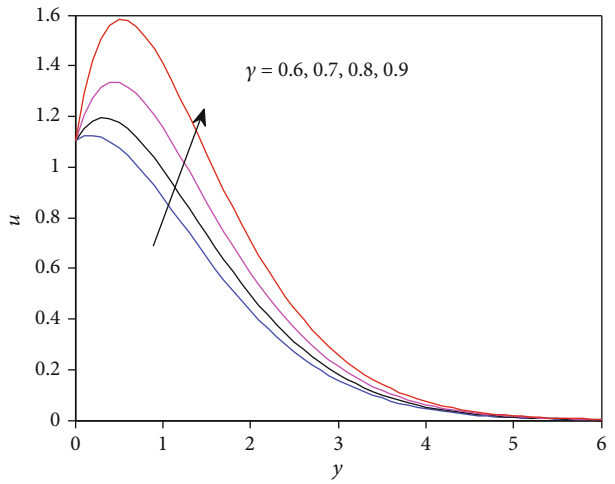

Figure 10: Newtonian heating impact on fluid velocity.

Newtonian heating refers to the process of heat exchange in which internal resistance is minimal in comparison to the plate's wall or surface resistance. That is why there has been a greater change in surface temperature. As a result, when Newtonian heating increases, the temporal distribution at the surface increases. In this line, increasing temperature also results in increased fluid acceleration, which causes an increment in velocity profiles including thickness of momentum boundary layer. With the aid of this idea, one may comprehend how the supplied system's velocity profile and temperature distribution increase when this parameter rises, as seen in Figures 10 and 11.

The surface of mass in transit and the product of the varying driving force concentration can be used to calculate the mass transfer coefficient. Anyone can deduce the straight-forward relation of conjugate parameter, concentration, and mass transfer coefficient from this expression. As a result, as this parameter rises, the species concentration and hence the thickness of the solutal boundary layer rise, while the fluid velocity and thickness of the boundary layer due to momentum decrease (see Figures 12 and 13).

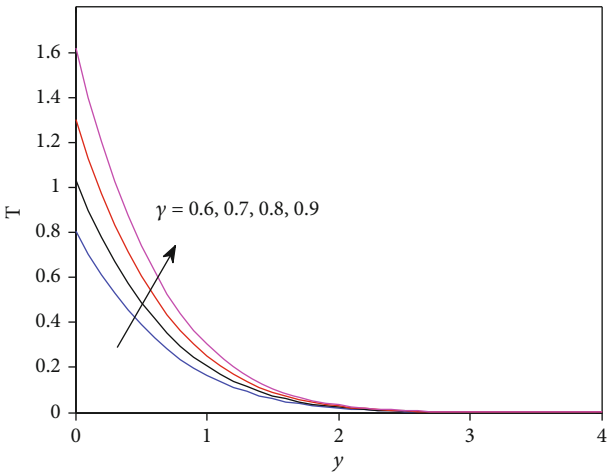

Figure 11: Newtonian heating effect on fluid temperature.

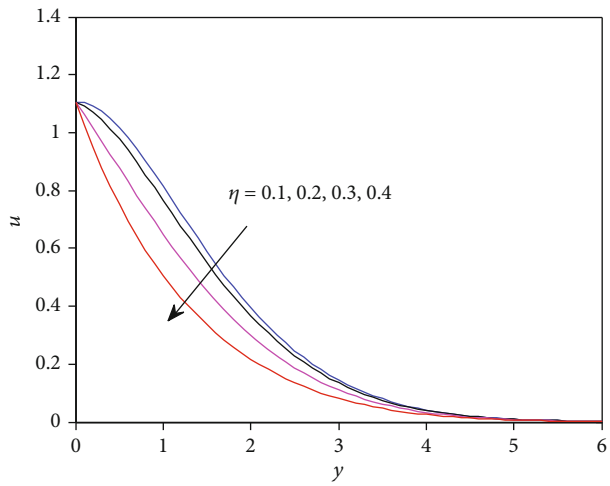

Figure 12: Impacts of mass transfer coefficient on velocity.

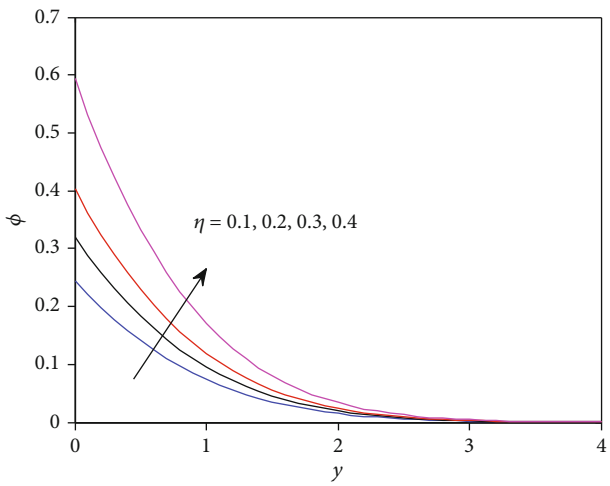

Figure 13: Impacts of mass transfer coefficient on concentration.

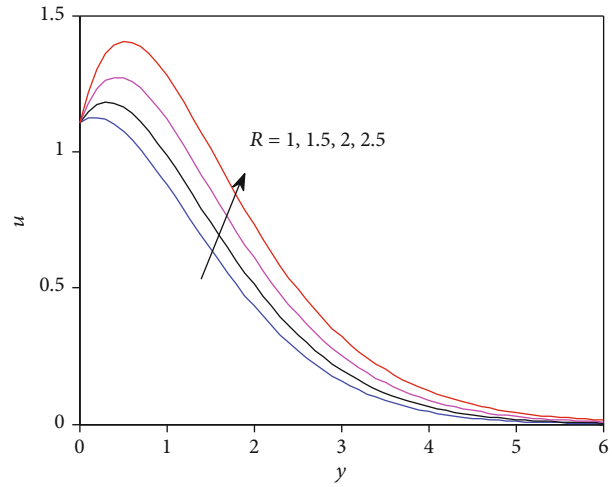

Figure 14: Thermal radiation effect on fluid velocity.

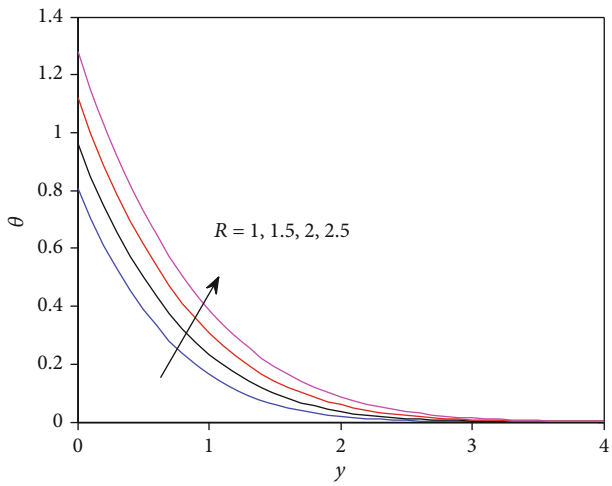

Figure 15: Thermal radiation effect on fluid temperature.

Figures 14 and 15 show how thermal radiation affects temperature and dimensionless fluid velocity. Based on what is known about thermal science, thermal radiation is defined as energy emission in the form of moving subatomic particles or electromagnetic waves. Obviously, the temperature affects how much energy is released. The little amount of heat absorption is necessary when thermal radiation is transferred from one surface to another. Due to the presence of heat conduction or convection, the surface may also permit heat to escape to the surroundings. Therefore, fluid temperature can be thought of as a function of thermal radiation. As the thermal radiation parameter rises, the fluid velocity and temperature distribution do as well.

Thermal radiation influences on dimensionless fluid velocity including temperature have been illustrated in Figures 14 and 15. According to what is known about thermal science, thermal radiation is defined as energy emission in the form of moving subatomic particles or electromagnetic waves. Obviously, the temperature affects how much energy is released. The little amount of heat absorption is

Table 1: Shearing stress variations.

a	t	Gr	Gm	R	α	β	P_r	Sc	η	γ	τ
0.1	0.4	1	1	1	$\pi/3$	2	0.71	0.6	0.6	0.6	0.4371
0.2	0.4	1	1	1	$\pi/3$	2	0.71	0.6	0.6	0.6	0.5243
0.1	0.5	1	1	1	$\pi/3$	2	0.71	0.6	0.6	0.6	0.4124
0.1	0.6	1	1	1	$\pi/3$	2	0.71	0.6	0.6	0.6	0.3643
0.1	0.4	2	1	1	$\pi/3$	2	0.71	0.6	0.6	0.6	0.1804
0.1	0.4	3	1	1	$\pi/3$	2	0.71	0.6	0.6	0.6	0.0520
0.1	0.4	1	2	1	$\pi/3$	2	0.71	0.6	0.6	0.6	0.3799
0.1	0.4	1	3	1	$\pi/3$	2	0.71	0.6	0.6	0.6	0.3228
0.1	0.4	1	1	2	$\pi/3$	2	0.71	0.6	0.6	0.6	0.2896
0.1	0.4	1	1	3	$\pi/3$	2	0.71	0.6	0.6	0.6	0.1183
0.1	0.4	1	1	1	$\pi/6$	2	0.71	0.6	0.6	0.6	0.2073
0.1	0.4	1	1	1	$\pi/4$	2	0.71	0.6	0.6	0.6	0.3071
0.1	0.4	1	1	1	$\pi/3$	3	0.71	0.6	0.6	0.6	0.4155
0.1	0.4	1	1	1	$\pi/3$	4	0.71	0.6	0.6	0.6	0.4030
0.1	0.4	1	1	1	$\pi/3$	2	0.81	0.6	0.6	0.6	0.4705
0.1	0.4	1	1	1	$\pi/3$	2	0.91	0.6	0.6	0.6	0.4959
0.1	0.4	1	1	1	$\pi/3$	2	0.71	0.7	0.6	0.6	0.7743
0.1	0.4	1	1	1	$\pi/3$	2	0.71	0.8	0.6	0.6	0.4359
0.1	0.4	1	1	1	$\pi/3$	2	0.71	0.6	0.7	0.6	0.3987
0.1	0.4	1	1	1	$\pi/3$	2	0.71	0.6	0.8	0.6	0.3635
0.1	0.4	1	1	1	$\pi/3$	2	0.71	0.6	0.6	0.7	0.3545
0.1	0.4	1	1	1	$\pi/3$	2	0.71	0.6	0.6	0.8	0.2501

necessary when thermal radiation propagates from one surface to another. Furthermore, because of the heat transfer by other means such as conduction or convection, the surface may permit heat to diffuse in its adjacent neighborhood depending on the ambient temperature. In light of this, fluid temperature can be thought of as a factor in thermal radiation. Due to the increased thermal radiation parameter, the fluid velocity and temperature distribution both rise. In this instance, the thermal and momentum boundary layer thicknesses expand together with the thermal radiation entity.

7.1. Analysis of Surface-Based Dimensionless Coefficients. Shearing stress numerical variations for numerous fundamental physical entities are shown in Table 1. As it is shown in this table, as a, α, and Pr increase, shearing stress also increases. However, it decreases as t, Gr, Gm, R, β, Sc, η, and γ grow. The most intriguing element in this situation is that when plate inclination increases, shearing stress or local skin friction reduces because of the significant friction created close to the plate's surface. Table 2 illustrates the effects of many significant physical parameter on heat transfer coefficient and mass transfer coefficient values. It is obvious that an increment in R, γ, and t results in a rise of the Nusselt number, whereas an increment in Pr results in a decrement in the Nusselt number, similar to how an increase in Sc, η, and t results in an increment of Sherwood's number.

Table 2: Mass and heat transfer rate variations.

R	P_r	γ	Sc	η	t	Nu	Sh
1	0.71	0.6	—	—	0.4	1.4809	—
2	0.71	0.6	—	—	0.4	1.9279	—
1	0.8	0.6	—	—	0.4	1.3707	—
1	1	0.6	—	—	0.4	1.2421	—
1	0.71	0.7	—	—	0.4	2.0750	—
1	0.71	0.8	—	—	0.4	2.9127	—
—	—	—	0.6	0.6	0.4	—	0.4038
—	—	—	0.8	0.6	0.4	—	1.1530
—	—	—	0.6	0.7	0.4	—	1.5343
—	—	—	0.6	0.8	0.4	—	2.0155
1	0.71	0.6	0.6	0.6	0.5	1.6797	1.2646
1	0.71	0.6	0.6	0.6	0.6	1.9074	1.3793

8. Conclusion

In this study, convective boundaries, viz., solutal and thermal boundary conditions, as well as the effects of heat and mass in transit, have been investigated in relation to radiative Casson fluid flow due to an exponentially accelerated slanted plate. The partial differential equations (PDEs) representing the flow problems are converted into ordinary

differential equations (ODEs) applying the Laplace transform. Following that, analytically determined closed-form solutions for fluid velocity, temperature, and concentration are produced. In graphs and tabular form, physical elements controlling the fluid flow behaviors are thoroughly examined. The following are the investigation's main findings:

(i) Increasing the plate inclination decreases fluid velocity while increasing skin friction

(ii) Local skin friction decreases when buoyant forces are exerted on the supplied fluid expand, but the Casson fluid velocity increases

(iii) Shearing stress rises as the Prandtl number rises, whereas the distribution of temperature, speed, and rate of heat transfer declines as the number rises

(iv) In contrast to shearing stress reduction, thermal radiation increases fluid velocity, heat transfer rate, and temperature

(v) Increased Casson fluid parameter results in increased velocity profiles and decreased local skin friction

(vi) Temperature and fluid velocity both rise with increasing mass transfer and Newtonian heating coefficients

(vii) With an increase of Newtonian heating and mass transfer coefficients, the shearing stress drops down while the Nusselt and Sherwood numbers rise up

This model can be extended to complex flows involving nonlinear partial differential equations. That is, we propose to extend this problem to the nonlinear case wherein the obtained solutions to the present linear case will be used as benchmark solutions to validate the approximate solutions obtained by the numerical methods to the proposed nonlinear case. We also propose to consider the effects of other physical entities such as fluid rotation, forced convection, and permeability of the medium in the future which are not considered in the present case. It is also advised that this investigation be expanded in further work by including terms for magnetic field, viscous dissipation, and Joule heating in the momentum and energy equation. Numerous technical and scientific applications make use of the magnetic field, viscous dissipation, and Joule heating terminology.

Nomenclature

R: Thermal radiation
Gr: Thermal Grashof number
q: Fluid velocity (m/s)
C: Fluid concentration (kmol/m^3)
ν: Viscosity (kinematic) (m^2/s)
β_T: Volumetric heat expansion (1/K)
g: Gravitational acceleration (m/s^2)
q_r: Radiative heat flux (W/m^2)
k_f: Mass transfer coefficient (kg/m^2 s)
q_o: Constant velocity of the wall (m/s)
α: Inclination angle of the plate
a': Dimensional accelerating parameter
θ: Dimensionless temperature
τ: Local skin friction
Sh: Sherwood number
γ: Newtonian heating parameter
t: Nondimensional time
β: Casson nanofluid parameter
Gm: Solutal Grashof number
T: Fluid temperature (K)
P_r: Prandtl number
ρ: Fluid density (kg/m^3)
β_C: Volumetric mass expansion (m^3/kg)
κ: Thermal conductivity (W/mK)
C_p: Specific heat capacity (J/kgK)
h_f: Heat transfer coefficient (W/m^2 K)
μ: Dynamic viscosity (kg/ms)
D_m: Mass diffusivity
t': Dimensional time (s)
ϕ: Dimensionless concentration
Nu: Nusselt number
a: Accelerating parameter
η: Conjugate parameter for concentration
Sc: Schmidt number.

Data Availability

The data used to support the findings of this study are included within the article. The data generated using MATLAB code is already presented in the tables and figures that are included in Results and Discussion of the manuscript.

Conflicts of Interest

The authors declare that they have no conflicts of interest.

References

[1] M. B. Riaz, A. Atangana, and N. Iftikhar, "Heat and mass transfer in Maxwell fluid in view of local and non-local differential operators," *Journal of Thermal Analysis and Calorimetry*, vol. 143, no. 6, pp. 4313–4329, 2021.

[2] M. F. Endalew and S. Sarkar, "Temporal analysis of dual phase-lag double-diffusive MHD flow within a porous microchannel with chemical reaction," *Heat Transfer-Asian Research*, vol. 48, no. 4, pp. 1292–1317, 2019.

[3] M. F. Endalew, S. Sarkar, G. S. Seth, and O. D. Makinde, "Dual-phase-lag heat transfer model in hydromagnetic second grade flow through a microchannel filled with porous material: a time-bound analysis," *Revue des Composites et des Materiaux Avances*, vol. 28, no. 2, pp. 173–194, 2018.

[4] S. Sarkar, M. F. Endalew, and O. D. Makinde, "Study of MHD second grade flow through a porous microchannel under the dual-phase-lag heat and mass transfer model," *Journal of Applied and Computational Mechanics*, vol. 5, no. 4, pp. 763–778, 2019.

[5] M. F. Endalew and A. Nayak, "Thermal radiation and inclined magnetic field effects on MHD flow past a linearly accelerated

inclined plate in a porous medium with variable temperature," *Heat Transfer-Asian Research*, vol. 48, no. 1, pp. 42–61, 2019.

[6] M. F. Endalew, A. Nayak, and S. Sarkar, "Flow past an oscillating slanted plate under the effects of inclined magnetic field, radiation, chemical reaction, and time-varying temperature and concentration," *International Journal of Fluid Mechanics Research*, vol. 47, no. 3, pp. 247–261, 2020.

[7] M. F. Endalew and S. Sarkar, "Incidences of aligned magnetic field on unsteady MHD flow past a parabolic accelerated inclined plate in a porous medium," *Heat Transfer*, vol. 50, no. 6, pp. 5865–5884, 2021.

[8] S. Das, B. Tarafdar, and R. N. Jana, "Hall effects on unsteady MHD rotating flow past a periodically accelerated porous plate with slippage," *European Journal of Mechanics - B/Fluids*, vol. 72, pp. 135–143, 2018.

[9] M. Sobamowo, A. Yinusa, and O. Makinde, "A study on the effects of inclined magnetic field, flow medium porosity and thermal radiation on free convection of Casson nanofluid over a vertical plate," *World Scientific News*, vol. 138, no. 1, pp. 1–64, 2019.

[10] M. M. Nandeppanavar, "Melting heat transfer analysis of non-Newtonian Casson fluid due to moving plate," *Engineering Computations*, vol. 35, no. 3, pp. 1301–1313, 2018.

[11] A. Zaib, K. Bhattacharyya, M. S. Uddin, and S. Shafie, "Dual solutions of non-Newtonian Casson fluid flow and heat transfer over an exponentially permeable shrinking sheet with viscous dissipation," *Modelling and Simulation in Engineering*, vol. 2016, Article ID 6968371, 8 pages, 2016.

[12] T. Hayat, S. Asad, and A. Alsaedi, "Flow of Casson fluid with nanoparticles," *Applied Mathematics and Mechanics*, vol. 37, no. 4, pp. 459–470, 2016.

[13] A. Hussanan, M. Z. Salleh, R. M. Tahar, and I. Khan, "Unsteady boundary layer flow and heat transfer of a Casson fluid past an oscillating vertical plate with Newtonian heating," *PLoS One*, vol. 9, no. 10, article e108763, 2014.

[14] N. A. Sheikh, D. L. C. Ching, I. Khan, D. Kumar, and K. S. Nisar, "A new model of fractional Casson fluid based on generalized Fick's and Fourier's laws together with heat and mass transfer," *Alexandria Engineering Journal*, vol. 59, no. 5, pp. 2865–2876, 2020.

[15] K. Ahmad, Z. Wahid, and Z. Hanouf, "Heat transfer analysis for Casson fluid flow over stretching sheet with Newtonian heating and viscous dissipation," *Journal of Physics: Conference Series*, vol. 1127, no. 1, article 012028, 2019.

[16] E. M. Arthur, I. Y. Seini, and L. B. Bortteir, "Analysis of Casson fluid flow over a vertical porous surface with chemical reaction in the presence of magnetic field," *Journal of Applied Mathematics and Physics*, vol. 3, no. 6, pp. 713–723, 2015.

[17] S. Sarkar and M. F. Endalew, "Effects of melting process on the hydromagnetic wedge flow of a Casson nanofluid in a porous medium," *Boundary Value Problems*, vol. 2019, no. 1, 2019.

[18] M. F. Endalew and S. Sarkar, "A numerical study of forced convection casson nanofluid flow past a wedge with melting process," in *ASME International Mechanical Engineering Congress and Exposition*, p. IMECE2020-23276, Portland, Oregon, 2020.

[19] M. Hamid, M. Usman, Z. Khan, R. Haq, and W. Wang, "Heat transfer and flow analysis of Casson fluid enclosed in a partially heated trapezoidal cavity," *International Communications in Heat and Mass Transfer*, vol. 108, article 104284, 2019.

[20] S. Das, A. Banu, and R. Jana, "Delineating impacts of non-uniform wall temperature and concentration on time-dependent radiation-convection of Casson fluid under magnetic field and chemical reaction," *World Journal of Engineering*, vol. 18, no. 5, pp. 780–795, 2021.

[21] M. Amjad, I. Zehra, S. Nadeem, and N. Abbas, "Thermal analysis of Casson micropolar nanofluid flow over a permeable curved stretching surface under the stagnation region," *Journal of Thermal Analysis and Calorimetry*, vol. 143, no. 3, pp. 2485–2497, 2021.

[22] S. Sarkar, R. N. Jana, and S. Das, "Time-dependent entropy analysis in magnetized Cu-Al2O3/ethylene glycol hybrid nanofluid flow due to a vibrating vertical plate," *Fluid Mechanics Research*, vol. 47, no. 5, pp. 419–443, 2020.

[23] J. R. Pattnaik, G. C. Dash, and S. Singh, "Radiation and mass transfer effects on MHD flow through porous medium past an exponentially accelerated inclined plate with variable temperature," *Ain Shams Engineering Journal*, vol. 8, no. 1, pp. 67–75, 2017.

[24] R. Muthucumaraswamy, K. Sathappan, and R. Natarajan, "Heat transfer effects on flow past an exponentially accelerated vertical plate with variable temperature," *Theoretical and Applied Mechanics*, vol. 35, no. 4, pp. 323–331, 2008.

[25] A. Singh and N. Kumar, "Free-convection flow past an exponentially accelerated vertical plate," *Astrophysics and Space Science*, vol. 98, no. 2, pp. 245–248, 1984.

[26] M. M. Nandeppanavar, M. C. Kemparaju, and N. Raveendra, "Double-diffusive free convective flow of Casson fluid due to a moving vertical plate with non-linear thermal radiation," *Journal of Engineering*, vol. 18, no. 1, 2021.

[27] M. Awais, T. Hayat, M. Nawaz, and A. Alsaedi, "Newtonian heating, thermal-diffusion and diffusion-thermo effects in an axisymmetric flow of a Jeffery fluid over a stretching surface," *Brazilian Journal of Chemical Engineering*, vol. 32, no. 2, pp. 555–561, 2015.

[28] V. Rajesh, "Effects of mass transfer on flow past an impulsively started infinite vertical plate with Newtonian heating and chemical reaction," *Journal of Engineering Physics and Thermophysics*, vol. 85, no. 1, pp. 221–228, 2012.

[29] M. Qasim, N. Riaz, D. Lu, and M. I. Afridi, "Mixed convection flow over a stretching sheet of variable thickness: analytical and numerical solutions of self-similar equations," *Heat Transfer*, vol. 49, no. 6, pp. 3882–3899, 2020.

[30] S. K. Nandy, "Analytical solution of MHD stagnation-point flow and heat transfer of Casson fluid over a stretching sheet with partial slip," *ISRN Thermodynamics*, vol. 2013, Article ID 108264, 9 pages, 2013.

[31] S. Mukhopadhyay, P. R. De, K. Bhattacharyya, and G. Layek, "Casson fluid flow over an unsteady stretching surface," *Ain Shams Engineering Journal*, vol. 4, no. 4, pp. 933–938, 2013.

[32] M. F. Endalew, "Analytical study of heat and mass transfer effects on unsteady Casson fluid flow over an oscillating plate with thermal and solutal boundary conditions," *Heat Transfer*, vol. 50, no. 6, pp. 6285–6299, 2021.

[33] M. F. Endalew, S. Sarkar, and G. S. Seth, "Convective and dissipative temporal flow of Casson nanofluid past a tilted plate in a porous medium with Navier's slip and slanted magnetic field," *International Journal*, vol. 12, no. 6, pp. 43–64, 2021.

[34] A. Hussanan, I. Khan, and S. Shafie, "An exact analysis of heat and mass transfer past a vertical plate with Newtonian

heating," *Journal of Applied Mathematics*, vol. 2013, Article ID 434571, 9 pages, 2013.

[35] R. Siegel, *Thermal Radiation Heat Transfer*, CRC Press, 2001.

[36] R. B. Hetnarski, "An algorithm for generating some inverse Laplace transforms of exponential form," *Zeitschrift für angewandte Mathematik und Physik ZAMP*, vol. 26, no. 2, pp. 249–253, 1975.

[37] R. Hetnarski, "On inverting the Laplace transforms connected with the error function," *Applicationes Mathematicae*, vol. 4, no. 7, pp. 399–405, 1963.